GEOLOGY | THE GEOLOGICAL SOCIETY OF AMERICA®

https://doi.org/10.1130/G48445.1

Manuscript received 28 September 2020
Revised manuscript received 27 February 2021
Manuscript accepted 28 March 2021

Erosion of the Himalaya-Karakoram recorded by Indus Fan deposits since the Oligocene

Han Feng[1], Huayu Lu[1]*, Barbara Carrapa[2], Hanzhi Zhang[1], Jun Chen[3], Ying Wang[1] and Peter D. Clift[4]
[1]School of Geography and Ocean Science, Nanjing University; Key Laboratory of Coast and Island Development, Ministry of Education, Nanjing 210023, China
[2]Department of Geosciences, University of Arizona, Tucson, Arizona 85721, USA
[3]School of Earth Sciences and Engineering, Nanjing University; Key Laboratory of Surficial Geochemistry, Ministry of Education, Nanjing 210023, China
[4]Department of Geology and Geophysics, Louisiana State University, Baton Rouge, Louisiana 70803, USA

ABSTRACT

The Cenozoic erosion history of the Himalaya-Karakoram, which is a function of tectonically driven uplift and monsoon climatic evolution in South Asia, remains elusive, especially prior to the Miocene. Here, we present a multiproxy geochemical and thermochronological analysis of the oldest samples available from the Arabian Sea, which we used to investigate the erosion history of the Himalayan and Karakoram orogenic system. The Indus Fan records rapid and sustained erosion of the Himalayan-Karakoram mountains from before 24 Ma (ca. 30) to ca. 16 Ma concurrent with changing provenance from the Indian (Himalayan) and Eurasian plates. Our data, combined with previous studies of younger Indus Fan deposits, indicate that the mid-to-late Cenozoic erosion history of the Himalayan-Karakoram mountains is overall consistent with a vigorous monsoonal climate from the late Oligocene to middle Miocene and with changes in global climate in the late Miocene, whereas erosion and deposition are relatively insensitive to changes in sources and rock erodibility. Although tectonic processes were active throughout, we suggest that the erosional signatures of the Himalayan-Karakoram mountains from the Indus Fan largely preserve a record of climate changes since the Oligocene.

INTRODUCTION

The Himalaya-Karakoram mountains form the highest topography on Earth and have experienced dramatic tectonic activity since the start of India-Eurasia continental collision, probably in the early Cenozoic (Hodges, 2000; Yin, 2006; Kapp and DeCelles, 2019). The uplift and unroofing of these high landforms have had a major impact on global and regional climate (Molnar et al., 1993), especially the South Asian monsoon, which in turn affects mountain building through surface erosion (Clift et al., 2008). The Neogene erosion of the Himalaya and Karakoram is partly documented by studies of the hinterland and foreland basins (e.g., Najman, 2006; Thiede et al., 2009; Stickroth et al., 2019), but the timing and extent of erosion of the Himalaya and Karakoram before the Miocene (>23 Ma) are poorly constrained (e.g., Qayyum et al., 2001). This limits our understanding of the history of erosion and of the interactions between tectonics and climate (e.g., Herman et al., 2013).

The Indus River, forming the second biggest submarine fan in the world (Fig. 1A), originates in the Himalayan and Karakoram orogenic belts, flows southward, and drains into the Arabian Sea (Fig. 1B). The oldest detritus in the Arabian Sea has been dated at approximately the middle and late Eocene (ca. 45 Ma; Clift et al., 2001), and it provides an excellent record of the early evolution history of Himalaya-Karakoram erosion. This study presents multiproxy provenance analysis and detrital apatite fission-track (AFT) dating of deep-sea sedimentary rocks to investigate the erosion/exhumation history of the Himalaya-Karakoram from Oligocene (>24 Ma) to middle Miocene (ca. 16 Ma) time.

GEOLOGICAL CONTEXT

The Indus Fan (Fig. 1A), located in the northwestern Arabian Sea, is composed of more than 11 km of clastic deposits that are mostly derived from the Indus River catchment, which drains the Himalaya-Karakoram mountains (Fig. 1B). Samples from sedimentary units recovered from Ocean Drilling Program (ODP) Sites 722 and 731 (Fig. 1C) on the western edge of the fan were the focus of this study. The lower parts of the drilled sections at Sites 722 and 731 were derived from the western Himalaya and Karakoram regions (Fig. 1B), delivered via the Indus River and through submarine turbidity currents (Clift et al., 2001). The turbidite sedimentary units are characterized by clear fining-upward sequences, showing a coarse-grained sandstone base and a siltstone or silty claystone cap, with bed thicknesses ranging from ~10 cm to as much as 150 cm (Shipboard Scientific Party, 1989a). The depositional ages of the analyzed samples were established based on biostratigraphy and paleomagnetism (Shipboard Scientific Party, 1989a, 1989b) and range from >24 Ma (younger than ca. 30 Ma) to ca. 16 Ma (see age controls in Fig. 1D and the Supplemental Material[1]).

The Indus River drains several major tectonic units belonging to the Indian and Eurasian plates (Fig. 1B), respectively. The Karakoram and Kohistan-Ladakh magmatic arc (KLA) dominate the Eurasian plate within the Indus drainage; both are characterized by zircon U-Pb ages mostly younger than 200 Ma (Fig. 2A), and by amphibole-dominated detrital heavy mineral assemblages (Fig. 3C; Liang et al., 2019). In addition, the KLA is characterized by less

*E-mail: huayulu@nju.edu.cn

[1]Supplemental Material. Analytical methods, age controls, data tables, and additional figures. Please visit https://doi.org/10.1130/GEOL.S.14582763 to access the supplemental material, and contact editing@geosociety.org with any questions.

CITATION: Feng, H., et al., 2021, Erosion of the Himalaya-Karakoram recorded by Indus Fan deposits since the Oligocene: Geology, v. 49, p. , https://doi.org/10.1130/G48445.1

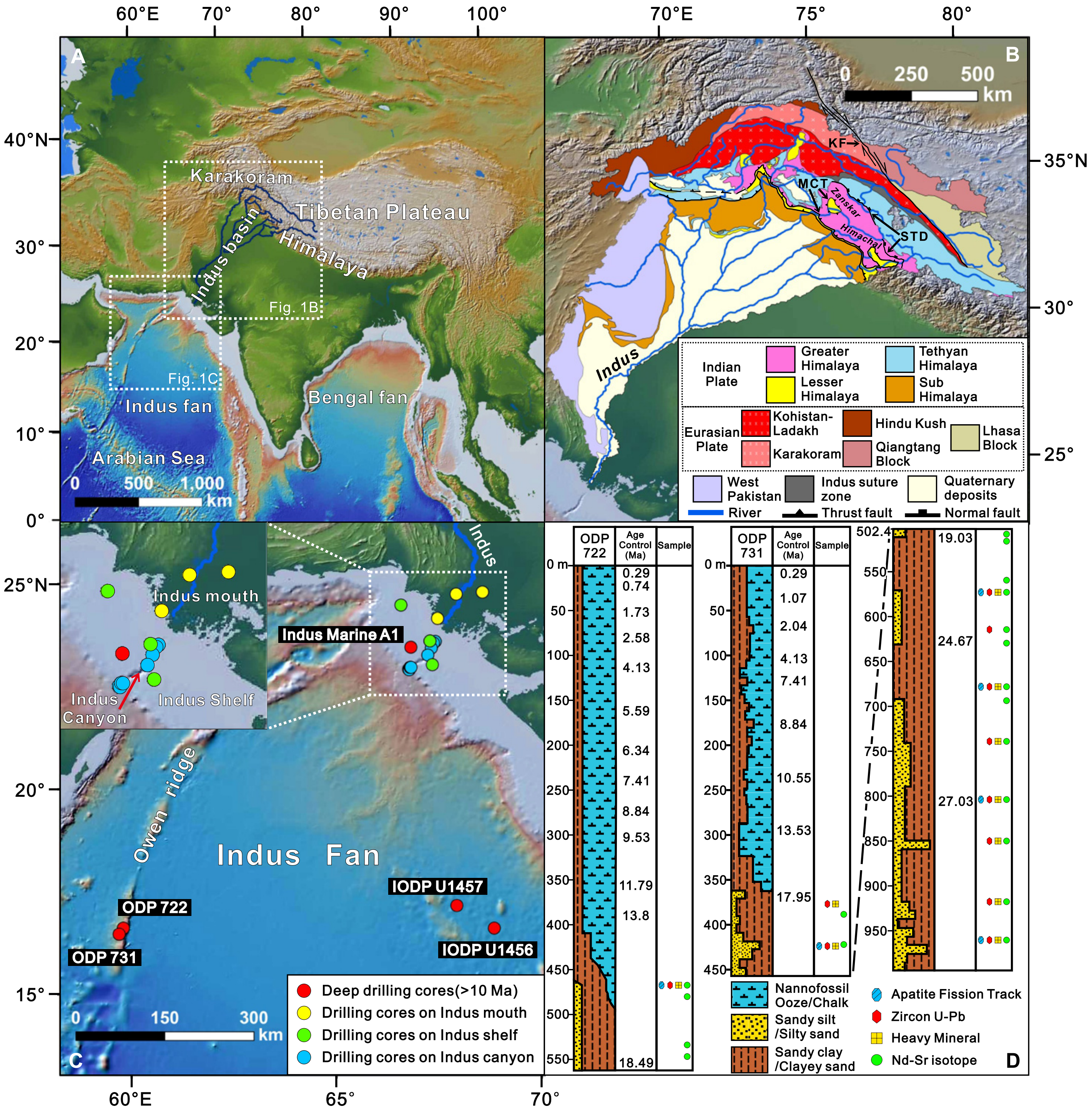

Figure 1. (A) Shaded relief map of South Asia and the Arabian Sea. (B) Tectonic units within the Indus drainage, including the Indian and Eurasian plates (from Yin, 2006). (C) Shaded relief map of the northwestern Arabian Sea, showing locations of ocean drilling sites and two study sites, Ocean Drilling Program (ODP) Site 722 (16°37′N, 59°48′E) and Site 731 (16°28′N, 59°42′E), from which we obtained samples. (D) Sedimentary logs of ODP 722 and 731 showing lithologies, age controls, and sample locations (see Tables S1 and S2 [see footnote 1]). STD—South Tibetan Detachment; MCT—Main Central Thrust; KF—Karakoram fault; IODP—International Ocean Discovery Program.

radiogenic ε_{Nd} and $^{87}Sr/^{86}Sr$ values than the Karakoram (Fig. 3A and 3B; Reichardt et al., 2010). The Himalaya are formed of metamorphic and sedimentary rocks originating on the Indian plate and consist of the Neoproterozoic or Ordovician to Paleocene Tethyan Himalayan Sequence (THS), the Neoproterozoic to Cambrian Greater Himalayan Sequence (GHS), and the mostly Paleoproterozoic Lesser Himalayan Sequence (LHS) (Fig. 1B). Although there are some lateral differences along the Himalaya, the GHS and THS have similar zircon U-Pb age distributions with major peaks ranging ca. 470–1100 Ma, ca. 1650–1800 Ma, and ca. 2400–2550 Ma in Zanskar, Himachal, and Nepal Himalaya (Figs. 1B and 2A; Gehrels et al., 2011; DeCelles et al., 2020). The GHS and THS also have similar ε_{Nd} and $^{87}Sr/^{86}Sr$ values, both of which are more radiogenic than those of the Eurasian plate (Fig. 3A and 3B; Robinson et al., 2001). The LHS is characterized by detrital zircon U-Pb ages with peaks at ca. 1800–1900 Ma and ca. 2500 Ma (Fig. 2A; Gehrels et al., 2011; DeCelles et al., 2020) and ε_{Nd} and $^{87}Sr/^{86}Sr$

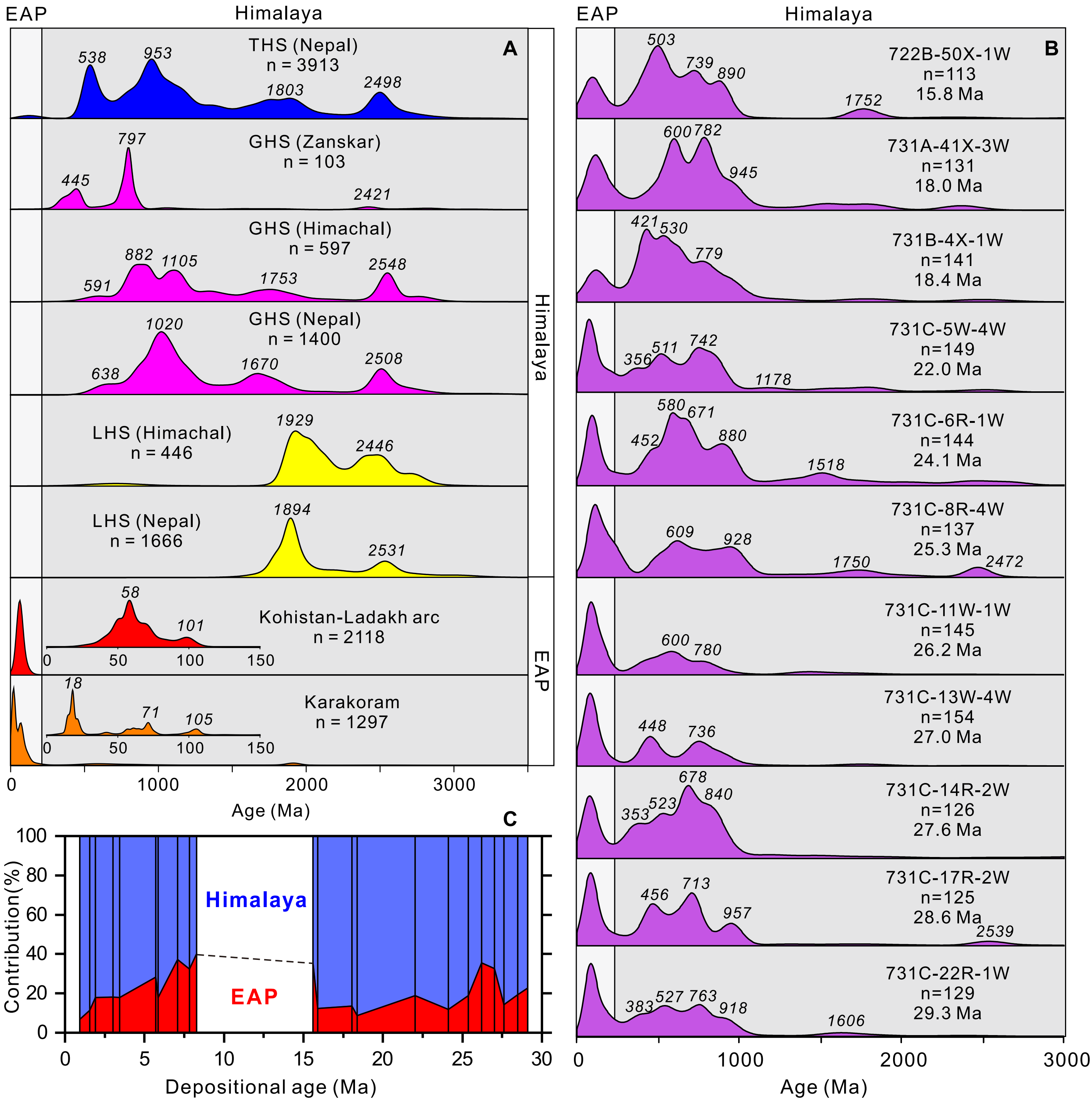

Figure 2. Zircon U-Pb age distributions for potential sources and samples with calculated source contributions. (A,B) Kernel density estimates for zircon age distributions of potential sources (A) (Table S9 [see footnote 1]) and samples from Ocean Drilling Program (ODP) Sites 722 and 731 (B) (Table S11). (C) Relative contributions of bulk materials from the Eurasian plate (EAP, zircon ages <200 Ma) and Himalaya (Indian plate, zircon ages >200 Ma) sedimentary sources, based on zircon U-Pb age populations (Table S6). Data <16 Ma are from Clift et al. (2019). THS—Tethyan Himalayan Sequence; GHS—Greater Himalayan Sequence; LHS—Lesser Himalayan Sequence.

values that are far more radiogenic than those of the other units (Figs. 3A and 3B; Robinson et al., 2001). Rivers draining Himalayan (GHS, THS, and LHS) source rocks carry fewer amphiboles and epidote but typically more garnet, ultrastable minerals (zircon, tourmaline, rutile [ZTR]), and high-grade minerals than those of the Eurasian plate (Fig. 3C; Liang et al., 2019).

RESULTS

Detrital zircon U-Pb ages of 11 samples (Fig. 2B), Sr-Nd isotope geochemistry of 19 samples (Fig. 3D), heavy mineral analysis of 10 samples (Fig. 3E), and detrital AFT data from six samples (Fig. 4A) from the lower part of the section recovered at ODP Sites 722 and 731 (>24–16 Ma) are presented here (Fig. 1D; also see analytical methods in the Supplemental Material).

The distributions of zircon U-Pb ages illustrate that most of the grains are within ca. 0–200 Ma and ca. 300–1000 Ma age ranges (Fig. 2B). The ε_{Nd} and $^{87}Sr/^{86}Sr$ values show relatively small variations from ca. 30 to 26 Ma (Fig. 3D), followed by a decrease in ε_{Nd} values

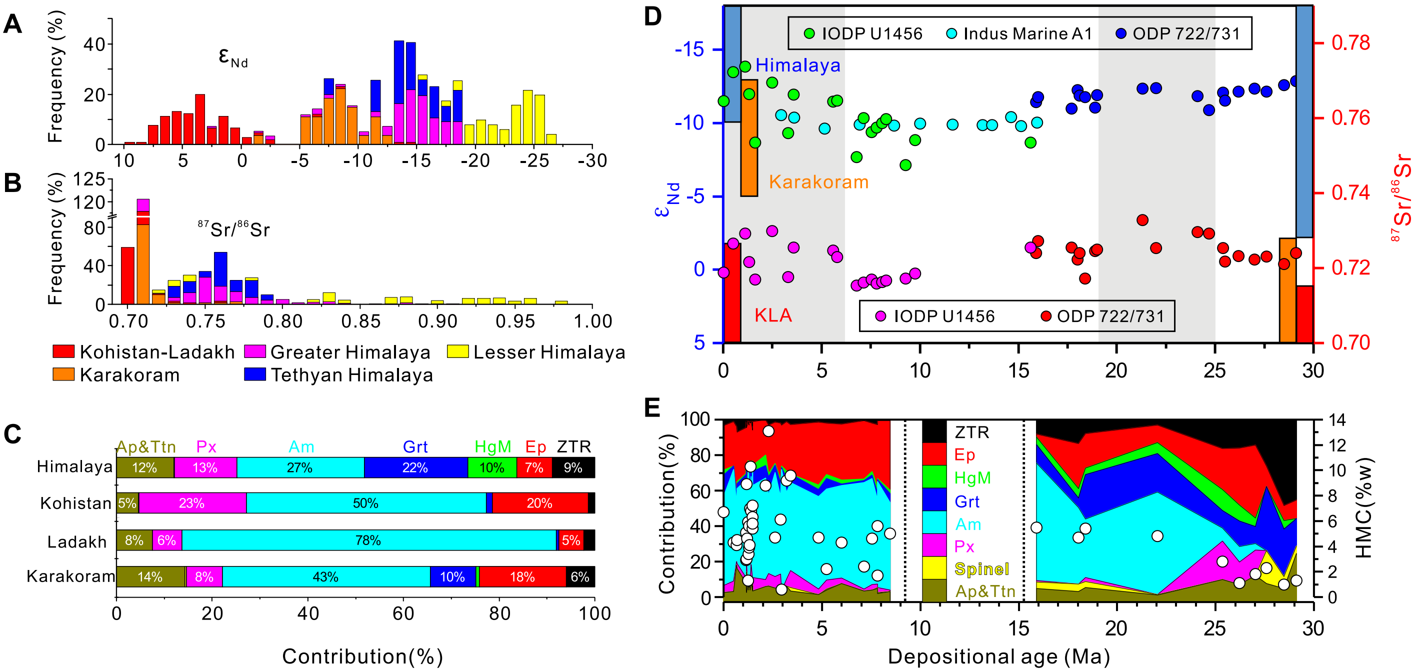

Figure 3. Sr-Nd isotopic compositions and heavy mineral assemblages for potential sources and samples. (A,B) ε_{Nd} and $^{87}Sr/^{86}Sr$ values for potential sources (Table S10 [see footnote 1]). (C) Detrital heavy mineral assemblages of potential sources (Table S3). "Himalaya" source includes the Greater Himalayan Sequence (GHS), Tethyan Himalayan Sequence (THS), and Lesser Himalayan Sequence (LHS). (D,E) Variations of Sr-Nd isotopic compositions and heavy mineral assemblages of Indus Fan deposits over the past ~30 m.y. (Tables S4 and S5). Data <16 Ma are from Andò et al. (2019), Garzanti et al. (2020), and Clift et al. (2008, 2019). ε_{Nd} and $^{87}Sr/^{86}Sr$ ranges of potential sources are shown as colored bars in D. High contributions from the Himalaya source at ca. 25–18 Ma and <6 Ma are indicated by the gray rectangle. Heavy mineral concentration of bulk sample (HMC) is represented by white circle in E. Ap—apatite; Ttn—titanite; Px—pyroxene; Am—amphibole; Grt—garnet; HgM—high-grade minerals (staurolite, andalusite, kyanite, sillimanite); Ep—epidote; ZTR—ultrastable minerals (zircon, tourmaline, and rutile). IODP—International Ocean Discovery Program; ODP—Ocean Drilling Program; KLA—Kohistan-Ladakh magmatic arc.

and an increase in $^{87}Sr/^{86}Sr$ values starting at ca. 25 Ma. The ε_{Nd} and $^{87}Sr/^{86}Sr$ records return to values similar to those recorded in ca. 30–26 Ma samples after ca. 18 Ma. Pyroxene appears in sediment younger than ca. 27 Ma; epidote and pyroxene remained high between ca. 27 and 25 Ma and decreased after ca. 25 Ma (Fig. 3E); amphibole first appeared at ca. 27 Ma and increased to peak values between ca. 22 Ma and ca. 16 Ma. Of the six samples analyzed for AFT thermochronology, five showed one single population, ranging from ca. 35.0 to 21.4 Ma

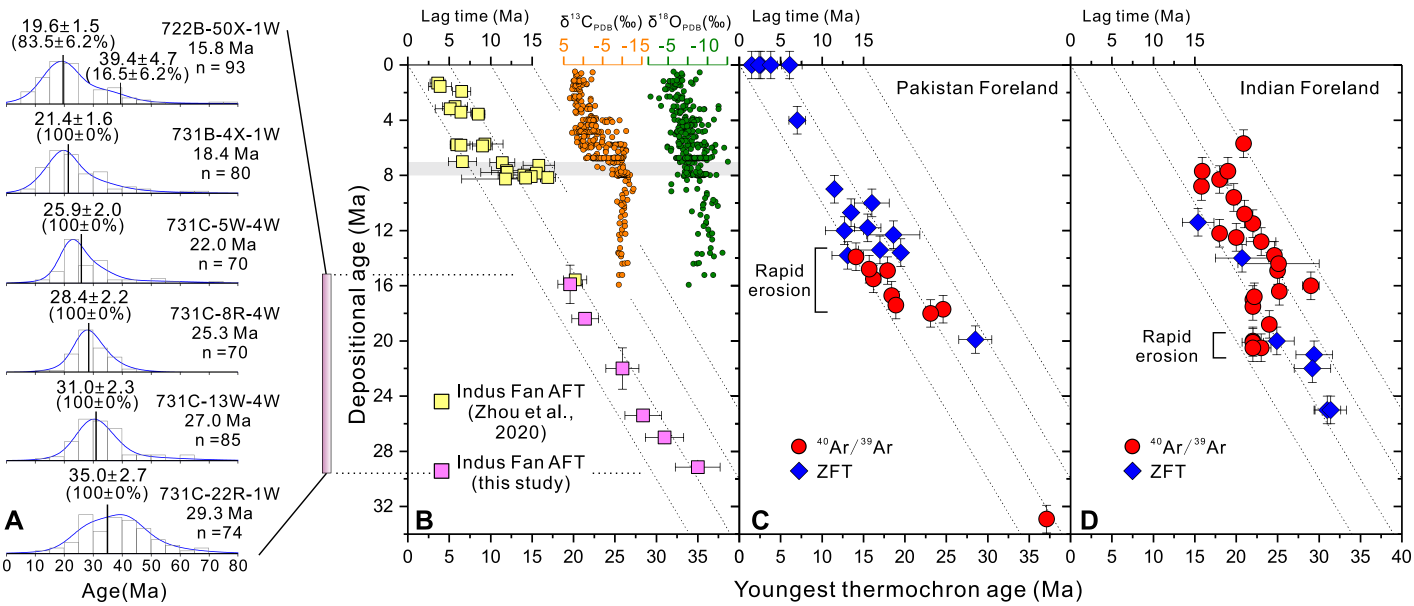

Figure 4. Thermochronological data for Indus Fan deposits and Himalayan foreland basin samples. (A) Kernel density estimates for apatite fission-track (AFT) ages (in Ma) of samples from Ocean Drilling Program (ODP) Sites 722 and 731 (Table S12 [see footnote 1]). (B–D) Lag-time plots of depositional age verus youngest thermochronological age peaks of samples from the Indus Fan (Table S8; Zhou et al., 2020) and Himalayan foreland basins. Light-gray bar indicates period of 8–7 Ma. Lag time data from the Pakistan and Indian foreland samples were compiled from Jain et al. (2009), Najman et al. (2009), Chirouze et al. (2015), and references therein. In B, $\delta^{13}C$ and $\delta^{18}O$ data are from pedogenic carbonates for deposits in South Asia (Table S13, and references therein). ZFT—zircon fission track; PDB—Peedee belemnite.

(Fig. 4A). The youngest sample (deposited at ca. 15.8 Ma) contained two populations with peak ages at ca. 19.6 Ma and ca. 39.4 Ma; the 19.6 Ma population accounts for 83.5% of the total (Fig. 4A).

DISCUSSION

Provenance Evolution of the Indus Fan

The sources of the Indus Fan sedimentary samples can be mainly divided into two groups (Fig. 2A): Eurasian Plate (EAP, including both the Karakoram and KLA, 0–200 Ma), and Himalaya (>200 Ma, including the GHS, THS, and LHS). Because the THS was originally deposited as a lateral equivalent of the GHS, it is difficult to distinguish between GHS and THS sources; the LHS, however, does not contain any zircons younger than ca. 1600 Ma and also produces more evolved Nd and Sr isotope signals (Fig. 2A; Gehrels et al., 2011; DeCelles et al., 2020). We estimated the total sediment budget based on the zircon age distributions of EAP and Himalayan sources with a correction using zircon fertilities for these two source groups (Fig. 2C; Table S6; Liang et al., 2019). The bulk budget indicates that the Indus Fan received more erosional materials from the Himalaya between ca. 25 and ca. 16 Ma (81%–91%) than before that time (Fig. 2C; Fig. S1). This is consistent with the ε_{Nd} and $^{87}Sr/^{86}Sr$ records, which show more Himalayan contribution between ca. 25 and ca. 18 Ma (Fig. 3D). The Himalayan detritus contribution was relatively low between ca. 16 and ca. 6 Ma (60%–68%), followed by a gradual increase after ca. 6 Ma (72%–93%) (Fig. 2C), as indicated by the zircon U-Pb ages and Sr-Nd isotope values from International Ocean Discovery Program (IODP) Site U1456 (Figs. 2C and 3D; Clift et al., 2019).

The high contribution of detritus from the Himalaya between ca. 25 and ca. 16 Ma can be partly explained by rapid unroofing of the GHS rocks and of their protoliths (Stickroth et al., 2019) in response to motion on the Main Central Thrust (MCT) and the South Tibetan Detachment (STD) (Fig. 1B; Hodges, 2000; Thiede et al., 2009), coupled with enhanced erosion (Clift et al., 2008). GHS prograde metamorphism ended by ca. 25 Ma (Kohn, 2014), followed by decompression and exhumation. Structural and sedimentological studies indicate that GHS rocks were likely not widely exposed before ca. 20 Ma (DeCelles et al., 2020; Stickroth et al., 2019), and possibly not until much later in the NW Himalaya (Webb, 2013), which implies that the geochemical signature from the ca. 25–20 Ma Indus detritus is a record of erosion of the overlying THS, which commenced no later than 45–40 Ma (Wiesmayr and Grasemann, 2002; Stickroth et al., 2019).

Initial motion of the Karakoram strike-slip fault (KF in Fig. 1B) at ca. 16 Ma (Phillips et al., 2013) might have triggered uplift and exhumation of local EAP rocks along this structure and changed the provenance of the Indus Fan. Miocene–Pliocene southward propagation of the Himalayan thrust front and development of the Lesser Himalaya duplex (LHD) between ca. 12 Ma and ca. 5 Ma (DeCelles et al., 2020) moved the locus of erosion to the south of the MCT. The increase in Himalayan contribution after ca. 6 Ma in the Indus Fan is consistent with final unroofing of the LHS, which is characterized by very negative ε_{Nd} and high $^{87}Sr/^{86}Sr$ values (Figs. 3A and 3B) (Najman et al., 2009; Clift et al., 2019).

The decreasing content of epidote and pyroxene in heavy mineral assemblages since ca. 25 Ma in Indus Fan sediments indicates less EAP but more Himalayan contributions (Fig. 3E). However, the increasing content of amphiboles suggests more contribution from EAP rocks between ca. 22 and ca. 16 Ma, which contrasts with the other provenance proxies discussed above. We suggest that the decreasing amphibole content in sediments older than ca. 22 Ma and the disappearance of both amphibole and pyroxene before ca. 27 Ma were mainly controlled by the impact of diagenesis (Andò et al., 2012) and not by a change in provenance. This is supported by the lower heavy mineral concentration values (Garzanti and Andò, 2007) in samples older than ca. 25 Ma (Fig. 3E), and by relatively constant heavy mineral assemblages in samples younger than ca. 9 Ma, which are not influenced by the provenance change starting at ca. 6 Ma (Figs. 2C, 3D, and 3E; Andò et al., 2019; Garzanti et al., 2020).

Erosion History of the Himalaya-Karakoram and Climatic Implications

All of the detrital AFT samples from >24–16 Ma Indus Fan deposits show similar patterns of late Eocene–Miocene detrital cooling age populations between ca. 39 and ca. 19 Ma (Fig. 4A). Detrital populations are older than the depositional age of the host strata and younger than the zircon U-Pb ages from the same samples (Fig. 2B). Combined with the observation that the oldest sample was collected from a depth of <1 km below the seafloor (Fig. 1D), this indicates that AFT ages represent cooling ages related to sediment source exhumation, rather than postdepositional thermal overprinting.

The lag time, defined as the time difference between the cooling age (in this case, the youngest detrital population) and the depositional age of a sample, represents the time elapsed from exhumation of the sample through its closure depth and final deposition (e.g., Bernet et al., 2001). Our results show that the lag times for the Indus Fan samples range from ∼6 m.y. to ∼3 m.y. (Fig. 4B), similar to the range measured at IODP Site U1456 (Zhou et al., 2020). This indicates relatively rapid and sustained erosion between >24 Ma and 16 Ma despite variations in tectonic activity, source, and rock erodibility (Figs. 2C and 3D). We suggest that the Indus Fan routing system has diluted local changes and sustained relatively rapid sediment delivery into the distal basin for millions of years. This requires significant discharge and hence a vigorous, e.g., monsoonal-type, climate (and relief) and active tectonics between >24 and 16 Ma. When analyzing published lag time data, we also observed a clear signal of rapid erosion (∼0 m.y. lag times) between ca. 20 and ca. 16 Ma (e.g., Pakistan and Indian forelands; Figs. 4C and 4D), which can be explained by rapid exhumation of the GHS, accompanied by a strong monsoon (Clift et al., 2008). A significant change in lag time at ca. 8–7 Ma (Fig. 4B) is not coupled with a change in source (Figs. 2C and 3D) and hence may, at least in part, reflect changes in climate. Stable isotope geochemistry from the Pakistan, Indian, and Nepal foreland basins shows increased aridity and seasonality of precipitation starting at ca. 8–7 Ma (Fig. 4B; e.g., Dettman et al., 2001), consistent with the transition from C_3 to C_4 vegetation occurring at the same time (Fig. 4B). An alternative interpretation of the ca. 8–7 Ma phase of rapid erosion could be the growth of the LHD and the resulting erosion of its cover unit (Najman et al., 2009). However, the LHD is suggested to have initiated no earlier than ca. 12 Ma and continued until ca. 5 Ma (DeCelles et al., 2020). Therefore, exhumation of the LHD alone cannot explain the increase in erosion as recorded by a change in lag time to ∼1–2 m.y. at ca. 8–7 Ma.

Although hotly debated, increasing erosion in the late Cenozoic is observed not only in cooling ages of the Indus Fan deposits (Fig. 4B), but also throughout the world (Herman et al., 2013), and it has been interpreted as the result of high-amplitude/high-frequency climate change (Zhang et al., 2001) and large-scale glacial erosion due to global cooling since ca. 8 Ma (Clift et al., 2008). Conversely, quasi-steady lag times, and by inference erosion, in the Himalaya-Karakoram during the late Oligocene to middle Miocene are here interpreted to be the result of low-amplitude/low-frequency climate change and relatively minor glacial erosion in response to a warmer and likely more humid climate compared to the late Cenozoic.

ACKNOWLEDGMENTS

This research was supported by the National Natural Science Foundation of China (grants 41888101, 41690111, and 42021001) and the International Ocean Discovery Program (IODP)–China. Samples were provided by the IODP, which are sincerely appreciated. We thank Peter G. DeCelles and Dhananjai K. Pandey for constructive criticisms on the manuscript.

REFERENCES CITED

Andò, S., Garzanti, E., Padoan, M., and Limonta, M., 2012, Corrosion of heavy minerals during weathering and diagenesis: A catalog for optical analysis: Sedimentary Geology, v. 280, p. 165–178, https://doi.org/10.1016/j.sedgeo.2012.03.023.

Andò, S., Aharonovich, S., Hahn, A., George, S.C., Clift, P.D., and Garzanti, E., 2019, Integrating heavy-mineral, geochemical and biomarker analyses of Plio-Pleistocene sandy and silty turbidites: A novel approach for provenance studies (Indus Fan, IODP Expedition 355): Geological Magazine, v. 157, p. 929–938, https://doi.org/10.1017/S0016756819000773.

Bernet, M., Zattin, M., Garver, J.I., Brandon, M.T., and Vance, J.A., 2001, Steady-state exhumation of the European Alps: Geology, v. 29, p. 35–38, https://doi.org/10.1130/0091-7613(2001)029<0035:SSEOTE>2.0.CO;2.

Chirouze, F., Huyghe, P., Chauvel, C., van der Beek, P., Bernet, M., and Mugnier, J.-L., 2015, Stable drainage pattern and variable exhumation in the Western Himalaya since the middle Miocene: The Journal of Geology, v. 123, p. 1–20, https://doi.org/10.1086/679305.

Clift, P.D., Shimizu, N., Layne, G.D., Blusztajn, J.S., Gaedicke, C., Schlüter, H.-U., Clark, M.K., and Amjad, S., 2001, Development of the Indus Fan and its significance for the erosional history of the Western Himalaya and Karakoram: Geological Society of America Bulletin, v. 113, p. 1039–1051, https://doi.org/10.1130/0016-7606(2001)113<1039:DOTIFA>2.0.CO;2.

Clift, P.D., Hodges, K.V., Heslop, D., Hannigan, R., Van Long, H., and Calves, G., 2008, Correlation of Himalayan exhumation rates and Asian monsoon intensity: Nature Geoscience, v. 1, p. 875–880, https://doi.org/10.1038/ngeo351.

Clift, P.D., Zhou, P., Stockli, D.F., and Blusztajn, J., 2019, Regional Pliocene exhumation of the Lesser Himalaya in the Indus drainage: Solid Earth, v. 10, p. 647–661, https://doi.org/10.5194/se-10-647-2019.

DeCelles, P.G., Carrapa, B., Ojha, T.P., Gehrels, G.E., and Collins, D., 2020, Structural and Thermal Evolution of the Himalayan Thrust Belt in Midwestern Nepal: Geological Society of America Special Paper 547, 77 p., https://doi.org/10.1130/2020.2547(01).

Dettman, D.L., Kohn, M.J., Quade, J., Ryerson, F.J., Ojha, T.P., and Hamidullah, S., 2001, Seasonal stable isotope evidence for a strong Asian monsoon throughout the past 10.7 m.y.: Geology, v. 29, p. 31–34, https://doi.org/10.1130/0091-7613(2001)029<0031:SSIEFA>2.0.CO;2.

Garzanti, E., and Andò, S., 2007, Heavy mineral concentration in modern sands: Implications for provenance interpretation, *in* Mange, M.A., and Wright, D.T., eds., Heavy Minerals in Use: Amsterdam, Netherlands, Elsevier, Developments in Sedimentology 58, p. 517–545, https://doi.org/10.1016/S0070-4571(07)58020-9.

Garzanti, E., Andò, S., and Vezzoli, G., 2020, Provenance of Cenozoic Indus Fan sediments (IODP Sites U1456 and U1457): Journal of Sedimentary Research, v. 90, p. 1114–1127, https://doi.org/10.2110/jsr.2019-195.

Gehrels, G., Kapp, P., DeCelles, P.G., Pullen, A., Blakey, R., Weislogel, A., Ding, L., Guynn, J., Martin, A., McQuarrie, N., and Yin, A., 2011, Detrital zircon geochronology of pre-Tertiary strata in the Tibetan-Himalayan orogen: Tectonics, v. 30, TC5016, https://doi.org/10.1029/2011TC002868.

Herman, F., Seward, D., Valla, P.G., Carter, A., Kohn, B., Willett, S.D., and Ehlers, T.A., 2013, Worldwide acceleration of mountain erosion under a cooling climate: Nature, v. 504, p. 423–426, https://doi.org/10.1038/nature12877.

Hodges, K.V., 2000, Tectonics of the Himalaya and southern Tibet from two perspectives: Geological Society of America Bulletin, v. 112, p. 324–350, https://doi.org/10.1130/0016-7606(2000)112<324:TOTHAS>2.0.CO;2.

Jain, A.K., Lal, N., Sulemani, B., Awasthi, A.K., Singh, S., Kumar, R., and Kumar, D., 2009, Detrital-zircon fission-track ages from the Lower Cenozoic sediments, NW Himalayan foreland basin: Clues for exhumation and denudation of the Himalaya during the India-Asia collision: Geological Society of America Bulletin, v. 121, p. 519–535, https://doi.org/10.1130/B26304.1.

Kapp, P., and DeCelles, P.G., 2019, Mesozoic–Cenozoic geological evolution of the Himalayan-Tibetan orogen and working tectonic hypotheses: American Journal of Science, v. 319, p. 159–254, https://doi.org/10.2475/03.2019.01.

Kohn, M.J., 2014, Himalayan metamorphism and its tectonic implications: Annual Review of Earth and Planetary Sciences, v. 42, p. 381–419, https://doi.org/10.1146/annurev-earth-060313-055005.

Liang, W., Garzanti, E., Andò, S., Gentile, P., and Resentini, A., 2019, Multimineral fingerprinting of Transhimalayan and Himalayan sources of Indus-derived Thal Desert sand (central Pakistan): Minerals (Basel), v. 9, p. 457, https://doi.org/10.3390/min9080457.

Molnar, P., England, P., and Martinod, J., 1993, Mantle dynamics, uplift of the Tibetan Plateau, and the Indian monsoon: Reviews of Geophysics, v. 31, p. 357–396, https://doi.org/10.1029/93RG02030.

Najman, Y., 2006, The detrital record of orogenesis: A review of approaches and techniques used in the Himalayan sedimentary basins: Earth-Science Reviews, v. 74, p. 1–72, https://doi.org/10.1016/j.earscirev.2005.04.004.

Najman, Y., Bickle, M., Garzanti, E., Pringle, M., Barfod, D., Brozovic, N., Burbank, D.W., and Andò, S., 2009, Reconstructing the exhumation history of the Lesser Himalaya, NW India, from a multitechnique provenance study of the foreland basin Siwalik Group: Tectonics, v. 28, TC5018, https://doi.org/10.1029/2009TC002506.

Phillips, R.J., Searle, M.P., and Parrish, R.R., 2013, The geochemical and temporal evolution of the continental lithosphere and its relationship to continental-scale faulting: The Karakoram fault, eastern Karakoram, NW Himalayas: Geochemistry Geophysics Geosystems, v. 14, p. 583–603, https://doi.org/10.1002/ggge.20061.

Qayyum, M., Niem, A.R., and Lawrence, R.D., 2001, Detrital modes and provenance of the Paleogene Khojak Formation in Pakistan: Implications for early Himalayan orogeny and unroofing: Geological Society of America Bulletin, v. 113, p. 320–332, https://doi.org/10.1130/0016-7606(2001)113<0320:DMAPOT>2.0.CO;2.

Reichardt, H., Weinberg, R.F., Andersson, U.B., and Fanning, C.M., 2010, Hybridization of granitic magmas in the source: The origin of the Karakoram Batholith, Ladakh, NW India: Lithos, v. 116, p. 249–272, https://doi.org/10.1016/j.lithos.2009.11.013.

Robinson, D.M., DeCelles, P.G., Patchett, P.J., and Garzione, C.N., 2001, The kinematic evolution of the Nepalese Himalaya interpreted from Nd isotopes: Earth and Planetary Science Letters, v. 192, p. 507–521, https://doi.org/10.1016/S0012-821X(01)00451-4.

Shipboard Scientific Party, 1989a, Site 722, *in* Prell, W.L., et al., Proceedings of the Ocean Drilling Program, Initial Reports, Volume 117: College Station, Texas, Ocean Drilling Program, p. 255–317, https://doi.org/10.2973/odp.proc.ir.117.107.1989.

Shipboard Scientific Party, 1989b, Site 731, *in* Prell, W.L., et al., Proceedings of the Ocean Drilling Program, Initial Reports, Volume 117: College Station, Texas, Ocean Drilling Program, p. 585–652, https://doi.org/10.2973/odp.proc.ir.117.108.1989.

Stickroth, S.F., Carrapa, B., DeCelles, P.G., Gehrels, G.E., and Thomson, S.N., 2019, Tracking the growth of the Himalayan fold-and-thrust belt from Lower Miocene foreland basin strata: Dumri Formation, western Nepal: Tectonics, v. 38, p. 3765–3793, https://doi.org/10.1029/2018TC005390.

Thiede, R.C., Ehlers, T.A., Bookhagen, B., and Strecker, M.R., 2009, Erosional variability along the northwest Himalaya: Journal of Geophysical Research, v. 114, F01015, https://doi.org/10.1029/2008JF001010.

Webb, A.A.G., 2013, Preliminary palinspastic reconstruction of Cenozoic deformation across the Himachal Himalaya (northwestern India): Geosphere, v. 9, p. 572–587, https://doi.org/10.1130/GES00787.1.

Wiesmayr, G., and Grasemann, B., 2002, Eohimalayan fold and thrust belt: Implications for the geodynamic evolution of the NW-Himalaya (India): Tectonics, v. 21, 1058, https://doi.org/10.1029/2002TC001363.

Yin, A., 2006, Cenozoic tectonic evolution of the Himalayan orogen as constrained by along-strike variation of structural geometry, exhumation history, and foreland sedimentation: Earth-Science Reviews, v. 76, p. 1–131, https://doi.org/10.1016/j.earscirev.2005.05.004.

Zhang, P., Molnar, P., and Downs, W.R., 2001, Increased sedimentation rates and grain sizes 2–4 Myr ago due to the influence of climate change on erosion rates: Nature, v. 410, p. 891–897, https://doi.org/10.1038/35073504.

Zhou, P., Carter, A., Li, Y., and Clift, P.D., 2020, Slowing rates of regional exhumation in the western Himalaya: Fission track evidence from the Indus Fan: Geological Magazine, v. 157, p. 848–863, https://doi.org/10.1017/S001675681900092X.

Printed in USA